Informatik aktuell

H. Handels T. M. Deserno
A. Maier K. H. Maier-Hein
C. Palm T. Tolxdorff
(Hrsg.)

Bildverarbeitung für die Medizin 2019

Algorithmen
Systeme
Anwendungen

Proceedings des Workshops vom 17. bis 19. März 2019 in Lübeck

Springer Vieweg

Informatik aktuell

Herausgegeben
im Auftrag der Gesellschaft für Informatik (GI)

Heinz Handels · Thomas M. Deserno
Andreas Maier · Klaus H. Maier-Hein
Christoph Palm · Thomas Tolxdorff
Herausgeber

Bildverarbeitung für die Medizin 2019

Algorithmen – Systeme – Anwendungen

Proceedings des Workshops
vom 17. bis 19. März 2019 in Lübeck

Springer Vieweg

Herausgeber

Heinz Handels
Universität zu Lübeck
Institut für Medizinische Informatik
Ratzeburger Allee 160, 23562 Lübeck

Thomas M. Deserno, geb. Lehmann
Technische Universität Braunschweig
und Medizinische Hochschule Hannover
Peter L. Reichertz Institut für Medizinische Informatik
Mühlenpfordtstr. 23, 38106 Braunschweig

Andreas Maier
Friedrich-Alexander-Universität
Erlangen-Nürnberg
Lehrstuhl für Mustererkennung
Martensstr. 3, 91058 Erlangen

Klaus H. Maier-Hein, geb. Fritzsche
Deutsches Krebsforschungszentrum (DKFZ)
Medical Image Computing E230
Im Neuenheimer Feld 581, 69120 Heidelberg

Christoph Palm
Ostbayerische Technische Hochschule
Regensburg
Fakultät für Informatik und Mathematik
Galgenbergstr. 32, 93053 Regensburg

Thomas Tolxdorff
Charité – Universitätsmedizin Berlin
Institut für Medizinische Informatik
Hindenburgdamm 30, 12200 Berlin

ISSN 1431-472X
Informatik aktuell
ISBN 978-3-658-25325-7 ISBN 978-3-658-25326-4 (eBook)
https://doi.org/10.1007/978-3-658-25326-4

Die Deutsche Nationalbibliothek verzeichnet diese Publikation in der Deutschen Nationalbibliografie; detaillierte bibliografische Daten sind im Internet über http://dnb.d-nb.de abrufbar.

CR Subject Classification (1998): A.0, H.3, I.4, I.5, J.3, H.3.1, I.2.10, I.3.3, I.3.5, I.3.7, I.3.8, I.6.3

Springer Vieweg

Springer Vieweg ist Teil von Springer Nature
Springer Vieweg ist ein Imprint der eingetragenen Gesellschaft Springer Fachmedien Wiesbaden GmbH und ist ein Teil von Springer Nature.
Die Anschrift der Gesellschaft ist: Abraham-Lincoln-Str. 46, 65189 Wiesbaden, Germany

Bildverarbeitung für die Medizin 2019

Veranstalter

IMI	Institut für Medizinische Informatik, Universität zu Lübeck

Unterstützende Fachgesellschaften

BVMI	Berufsverband Medizinischer Informatiker
CURAC	Computer- und Roboterassistierte Chirurgie
DAGM	Deutsche Arbeitsgemeinschaft für Mustererkennung
DGBMT	Fachgruppe Medizinische Informatik der Deutschen Gesellschaft für Biomedizinische Technik im Verband Deutscher Elektrotechniker
GI	Gesellschaft für Informatik – Fachbereich Informatik in den Lebenswissenschaften
GMDS	Gesellschaft für Medizinische Informatik, Biometrie und Epidemiologie
IEEE	Joint Chapter Engineering in Medicine and Biology, German Section

Tagungsvorsitz

Prof. Dr. rer. nat. habil. Heinz Handels
Institut für Medizinische Informatik, Universität zu Lübeck

Tagungssekretariat

Susanne Petersen
Institut für Medizinische Informatik
Ratzeburger Allee 160, Gebäude 64
23562 Lübeck
Tel: +49 451 3101 5601
Fax: +49 451 3101 5604
Email: vm2019@imi.uni-luebeck.de
Web: http://bvm-workshop.org

Lokale BVM-Organisation

Dr. Jan Ehrhardt
Prof. Dr. Heinz Handels (Leitung)
Prof. Dr. Mattias Heinrich
Susanne Petersen
Dr. Jan Wrage
und weitere Mitarbeiterinnen und Mitarbeiter des Instituts für Medizinische Informatik der Universität zu Lübeck

Verteilte BVM-Organisation

Prof. Dr. Thomas M. Deserno, Sven Neumann, Aaron Wiora, Jamie-Céline Heinzig, Noah Maxen, Björn Bajor, Peter Reichert, Aleksej Hecht, Hendrik Griesche – Peter L. Reichertz Institut für Medizinische Informatik, Technische Universität Braunschweig (Tagungsband)
Prof. Dr. Heinz Handels, Dr. Jan-Hinrich Wrage – Institut für Medizinische Informatik, Universität zu Lübeck (Beitragsbegutachtung)
Prof. Dr. Andreas Maier – Pattern Recognition Lab, Technische Fakultät der FAU – Nürnberg (Social Media, Special Issue)
Priv. – Doz. Dr. Klaus Maier – Hein, Jens Petersen – Division of Medical Image Computing, Deutsches Krebsforschungszentrum (DKFZ) (Anmeldung, Mailingliste)
Prof. Dr. Christoph Palm, Dr. Alexander Leis, Leonard Klausmann, Sümeyye R. Yildiran – Regensburg Medical Image Computing (ReMIC), OTH Regensburg (Internetpräsenz, Newsletter, Social Media)
Prof. Dr. Thomas Tolxdorff, Dr. Thorsten Schaaf – Institut für Medizinische Informatik, Charité – Universitätsmedizin Berlin (Internetpräsenz)

BVM-Komitee

Prof. Dr. Thomas M. Deserno, Peter L. Reichertz Institut für Medizinische Informatik, Technische Universität Braunschweig
Prof. Dr. Heinz Handels, Institut für Medizinische Informatik, Universität zu Lübeck
Prof. Dr. Andreas Maier, Pattern Recognition Lab, FAU Erlangen-Nürnberg
Priv.-Doz. Dr. Klaus Maier-Hein, Division of Medical Image Computing, DKFZ
Prof. Dr. Christoph Palm, Regensburg Medical Image Computing, OTH Regensburg
Prof. Dr. Thomas Tolxdorff, Institut für Medizinische Informatik,
Charité – Universitätsmedizin Berlin

Programmkommitee

Prof. Dr. Jörg Barkhausen, Universitätsklinikum Schleswig-Holstein Campus Lübeck
Priv.-Doz. Dr. Jürgen Braun, Charité-Universitätsmedizin Berlin
Prof. Dr. Thorsten Buzug, Universität zu Lübeck
Dr. Stefanie Demirci, TU München
Prof. Dr. Thomas Deserno, TU Braunschweig
Prof. Dr. Hartmut Dickhaus, Universität Heidelberg
Dr. Jan Ehrhardt, Universität zu Lübeck
Dr. Ralf Floca, DKFZ Heidelberg
Prof. Dr. Nils Forkert, University of Calgary, Canada
Prof. Dr. Horst Hahn, Fraunhofer MEVIS, Bremen

Sponsoren des Workshops BVM 2019

Die BVM wäre ohne die finanzielle Unterstützung der Industrie in ihrer erfolgreichen Konzeption nicht durchführbar. Deshalb freuen wir uns sehr über langjährige kontinuierliche Unterstützung mancher Firmen sowie auch über das neue Engagement anderer:

Gold-Sponsoren

Euroimmun AG
Seekamp 31, 23560 Lübeck
www.euroimmun.de

ID GmbH & Co KGaA
Platz vor dem Neuen Tor 2, 10115 Berlin
www.id-berlin.de

VisiConsult X-ray Systems & Solutions GmbH
Brandenbrooker Weg 2-4, 23617 Stockelsdorf
visiconsult.de

Silber-Sponsoren

Agfa HealthCare GmbH
Konrad-Zuse-Platz 1-3, 53185 Bonn
global.agfahealthcare.com

Haption GmbH
Dennewartstraße 25, 52068 Aachen
www.haption.de

Ibeo Automotive Systems GmbH
Merkurring 60-62, 22143 Hamburg
www.ibeo-es.com

Sponsoren

Medneo GmbH
Hausvogteiplatz 12, 10117 Berlin
www.medneo.com

MiE medical imaging electronics GmbH
Hauptstraße 112, 23845 Seth
mie-scintron.com

Beste wissenschaftliche Arbeiten

1. Maximilian Blendowski (Universität zu Lübeck)
   Blendowski M, Heinrich MP: 3D-CNNs for Deep Binary Descriptor Learning in Medical Volume Data

2. Hristina Uzunova (Universität zu Lübeck)
   Uzunova H, Handels H, Ehrhardt J: Unsupervised Pathology Detection in Medical Images using Learning-based Methods

3. Maike Stöve (Friedrich-Alexander-Universität Erlangen)
   Stoeve M, Aubreville M, Oetter N, Knipfer C, Neumann H, Stelzle F, Maier A: Motion Artifact Detection in Confocal Laser Endomicroscopy Images

Beste Präsentationen:

Weilin Fu (Friedrich-Alexander-Universität Erlangen)
Fu W, Breininger K, Schaffert R, Ravikumar N, Würfl T, Fujimoto J, Moult E, Maier A: Frangi-Net

Bestes Poster

André Klein (DKFZ Heidelberg)
Klein A, Warszawski J, Hillengaß J, Maier-Hein KH: Towards Whole-body CT Bone Segmentation

Vorwort

In diesem Jahr wird die Tagung Bildverarbeitung für die Medizin (BVM 2019) vom Institut für Medizinische Informatik an der Universität zu Lübeck ausgerichtet. Nach der erfolgreichen Durchführung der BVM 2001, 2011 und 2015 findet diese zentrale Tagung zu neuen Entwicklungen in der Medizinischen Bildverarbeitung in Deutschland nun zum vierten Mal in der traditionsreichen Hansestadt Lübeck statt.

Die medizinische Bildverarbeitung ist eine Schlüsseltechnologie in verschiedenen medizinischen Bereichen wie der Diagnoseunterstützung, der OP-Planung sowie der bildgeführten Chirurgie und Strahlentherapie. Methodisch haben hierbei in den letzten Jahren insbesondere Deep Neural Networks deutliche Fortschritte in Bezug auf Genauigkeit und Geschwindigkeit der Bildverarbeitungsverfahren ermöglicht, wobei das Potenzial maschineller Lernverfahren und Methoden der künstlichen Intelligenz im Bereich der Medizinischen Bildverarbeitung bei weitem noch nicht ausgeschöpft ist.

An der Universität zu Lübeck bilden die Medizinische Bildgebung und Bildverarbeitung einen zentralen universitären Forschungsschwerpunkt, der in den letzten Jahren systematisch ausgebaut wurde. Zudem bildet die Medizinische Bildverarbeitung in den Bachelor- und Masterstudiengängen Medizinische Informatik, Medizinische Ingenieurwissenschaften und Mathematik in Medizin und Lebenswissenschaften eine wichtige Vertiefungsrichtung. Vor diesem Hintergrund ist es eine besondere Freude, die BVM 2019 in Lübeck ausrichten zu dürfen.

Die BVM hat sich als ein zentrales interdisziplinäres Forum für die Präsentation und Diskussion von Methoden, Systemen und Anwendungen im Bereich der Medizinischen Bildverarbeitung etabliert. Ziel der Tagung ist die Darstellung aktueller Forschungsergebnisse und die Vertiefung der Gespräche zwischen Wissenschaftlern, Industrie und Anwendern. Die BVM richtet sich ausdrücklich auch an Nachwuchswissenschaftler, die über ihre Bachelor-, Master-, Promotions- und Habilitationsprojekte berichten wollen.

Die BVM 2019 wird unter der Federführung von Prof. Dr. rer. nat. habil. Heinz Handels, Direktor des Instituts für Medizinische Informatik der Universität zu Lübeck, ausgerichtet. Die Organisation ist wie in den letzten Jahren auf Fachkollegen aus Berlin, Braunschweig, Erlangen, Heidelberg, Lübeck und Regensburg verteilt, so dass die Organisatoren der vergangenen Jahre ihre Erfahrungen hier mit einfließen lassen können.

Anhand anonymisierter Bewertungen durch jeweils drei Fachgutachter wurden aus 87 eingereichten Beiträgen 28 Vorträge, 45 Poster und 2 Softwaredemonstrationen zur Präsentation ausgewählt. Die Qualität der eingereichten Arbeiten war insgesamt sehr hoch. Die besten Arbeiten werden auch in diesem Jahr mit BVM-Preisen ausgezeichnet. Die schriftlichen Langfassungen der Beiträge sind im Tagungsband zusammengefasst, der auch dieses Jahr wieder im Springer Verlag in der Reihe Informatik aktuell zur BVM erscheint. Das Programm wird durch eingeladene Gastvorträge zu aktuellen Themen des Deep

Learnings in der Medizinischen Bildverarbeitung sowie zur Beleuchtung und Diskussion der Sicht des Radiologen auf die aktuellen Entwicklungen abgerundet.

Die Internetseiten des Workshops bieten ausführliche Informationen über das Programm und organisatorische Details rund um die BVM 2019. Sie sind abrufbar unter der Adresse:

http://www.bvm-workshop.org

Am Tag vor dem wissenschaftlichen Programm werden drei Tutorials angeboten, bei denen in diesem Jahr verschiedene Aspekte der Deep Learnings in der Medizinischen Bildverarbeitung beleuchtet werden: Prof. Dr.-Ing. habil. Andreas Maier von der Friedrich-Alexander-Universität Erlangen-Nürnberg hält gemeinsam mit seinen Mitarbeiterinnen und Mitarbeitern ein Tutorial zum Thema „Deep Learning: Fundamentals“ ab. Hier wird eine Einführung in die grundsätzlichen Methoden des Deep Learnings und Ihre Anwendung auf medizinische Bilder gegeben. Fortgeschrittene Methoden des Deep Learnings in der Medizinischen Bildverarbeitung stehen im zweiten Tutorial mit dem Titel „Advanced Deep Learning Methods“ im Vordergrund, das von PD Dr. Klaus Maier-Hein und seinem Team vom DKFZ Heidelberg durchgeführt wird. Ergänzt wird dieses Angebot durch das dritte Tutorial „Hands-on Deep Learning in Pytorch“, das von Prof. Dr. Mattias Heinrich von der Universität zu Lübeck und seinem Team durchgeführt wird. Hier erhalten die Teilnehmenden Anleitungen zum praktischen Einsatz von neuesten Deep Learning Netzwerken und zur Handhabung der hierzu benötigten Softwarewerkzeuge.

Die Herausgeber dieser Proceedings möchten allen herzlich danken, die zum Gelingen der BVM 2019 beigetragen haben. Den Autoren für die rechtzeitige und formgerechte Einreichung ihrer qualitativ hochwertigen Arbeiten, dem Programmkomitee für die gründliche Begutachtung, den Gastrednern und den Referenten der Tutorials für Ihre aktive Mitgestaltung und inhaltliche Bereicherung der BVM 2019. Unser besonderer Dank gilt dem lokalen Organisationsteam in Lübeck, bestehend aus Dr. Jan Ehrhardt, Prof. Dr. Heinz Handels, Prof. Dr. Mattias Heinrich, Susanne Petersen und Dr. Jan Wrage, sowie den übrigen Mitarbeiterinnen und Mitarbeitern des Instituts für Medizinische Informatik in Lübeck, die durch ihren engagierten Einsatz die Organisation und Durchführung der BVM 2019 in der vorliegenden Form erst möglich gemacht haben. Weiterhin möchten wir den Helferinnen und Helfern an den Instituten in Berlin, Braunschweig, Erlangen, Heidelberg und Regensburg für Ihre Unterstützung bei der Organisation der BVM 2019 in Lübeck danken. Für die finanzielle Unterstützung bedanken wir uns bei den Fachgesellschaften und der Industrie.

Wir wünschen allen Teilnehmerinnen und Teilnehmern der BVM 2019 lehrreiche Tutorials, viele anregende Vorträge, Gespräche an den Postern und in der

Industrieausstellung sowie interessante neue Kontakte zu Kolleginnen und Kollegen aus dem Bereich der Medizinischen Bildverarbeitung.

Januar 2019

Heinz Handels (Lübeck)
Thomas Deserno (Braunschweig)
Andreas Maier (Erlangen)
Klaus Maier-Hein (Heidelberg)
Christoph Palm (Regensburg)
Thomas Tolxdorff (Berlin)

Inhaltsverzeichnis

Die fortlaufende Nummer am linken Seitenrand entspricht den Beitragsnummern, wie sie im endgültigen Programm des Workshops zu finden sind. Dabei steht V für Vortrag, P für Poster und S für Softwaredemonstration.

Session 1: Segmentation and Prediction

V1 *Neher PF, Stieltjes B, Maier-Hein KH*: Abstract: Anchor-Constrained Plausibility 1

V2 *Hofmann J, Böge M, Gladysz S, Jutzi B*: Automatic Detection of Blood Vessels in Optical Coherence Tomography Scans 2

V3 *Rippel O, Truhn D, Thüring J, Haarburger C, Kuhl CK, Merhof D*: Prediction of Liver Function Based on DCE-CT 8

Session 2: Deep Learning: Learning Strategies and Adversarial Models

V4 *Paschali M, Conjeti S, Navarro F, Navab N*: Abstract: Adversarial Examples as Benchmark for Medical Imaging Neural Networks 14

V5 *Uzunova H, Schultz S, Handels H, Ehrhardt J*: Evaluation of Image Processing Methods for Clinical Applications 15

V6 *Huang Y, Würfl T, Breininger K, Liu L, Lauritsch G, Maier A*: Abstract: Some Investigations on Robustness of Deep Learning in Limited Angle Tomography 21

V7 *Isensee F, Petersen J, Klein A, Zimmerer D, Jaeger PF, Kohl S, Wasserthal J, Koehler G, Norajitra T, Wirkert S, Maier-Hein KH*: Abstract: nnU-Net: Self-adapting Framework for U-Net-Based Medical Image Segmentation 22

V8 *Bouteldja N, Merhof D, Ehrhardt J, Heinrich MP*: Deep Multi-Modal Encoder-Decoder Networks for Shape Constrained Segmentation and Joint Representation Learning 23

V9 *Syben C, Stimpel B, Lommen J, Würfl T, Dörfler A, Maier A*: Abstract: Fan-to-Parallel Beam Conversion 29

Postersession 1:

Segmentation (Poster)

P1 *Wasserthal J, Neher PF, Maier-Hein KH*: Abstract: Tract Orientation Mapping for Bundle-Specific Tractography 30

P2 *Hille G, Dünnwald M, Becker M, Steffen J, Saalfeld S, Tönnies K*: Segmentation of Vertebral Metastases in MRI Using an U-Net like Convolutional Neural Network 31

P3 *Krauth J, Gerlach S, Marzahl C, Voigt J, Handels H*: Synthetic Training with Generative Adversarial Networks for Segmentation of Microscopies 37

P4 *Pham DD, Dovletov G, Warwas S, Landgraeber S, Jäger M, Pauli J*: Gradient-Based Expanding Spherical Appearance Models for Femoral Model Initialization in MRI 43

P5 *Pham DD, Dovletov G, Warwas S, Landgraeber S, Jäger M, Pauli J*: Deep Segmentation Refinement with Result-Dependent Learning ... 49

P6 *Al-Dhamari I, Bauer S, Paulus D, Hilal R, Lissek F, Jacob R*: Abstract: Automatic Estimation of Cochlear Duct Length and Volume Size 55

P7 *Amrehn M, Strumia M, Kowarschik M, Maier A*: Interactive Neural Network Robot User Investigation for Medical Image Segmentation 56

P8 *Nolden M, Schubert N, Schmitz D, Müller A, Axer M*: Tracing of Nerve Fibers Through Brain Regions of Fiber Crossings in Reconstructed 3D-PLI Volumes 62

P9 *Folle L, Vesal S, Ravikumar N, Maier A*: Dilated Deeply Supervised Networks for Hippocampus Segmentation in MRI 68

P10 *Lucas C, Schöttler JJ, Kemmling A, Aulmann LF, Heinrich MP*: Automatic Detection and Segmentation of the Acute Vessel Thrombus in Cerebral CT 74

P11 *Schnurr A-K, Schad LR, Zöllner FG*: Sparsely Connected Convolutional Layers in CNNs for Liver Segmentation in CT 80

P12 *Maier J, Black M, Hall M, Choi J-H, Levenston M, Gold G, Fahrig R, Eskofier B, Maier A*: Smooth Ride: Low-Pass Filtering of Manual Segmentations Improves Consensus 86

Denoising and Imange Enhancement (Poster)

P13 *Zarei S, Stimpel B, Syben C, Maier A*: User Loss 92

P14 *Koppers S, Coussoux E, Romanzetti S, Reetz K, Merhof D*: Sodium Image Denoising Based on a Convolutional Denoising Autoencoder 98

P15 *Kordon F, Lasowski R, Swartman B, Franke J, Fischer P, Kunze H*: Improved X-Ray Bone Segmentation by Normalization and Augmentation Strategies 104

P16 *Stimpel B, Syben C, Schirrmacher F, Hoelter P, Dörfler A, Maier A*: Multi-Modal Super-Resolution with Deep Guided Filtering 110

Registration and Motion Correction (Poster)

P17 *Chen S, Gehrer S, Kaliman S, Ravikumar N, Becit A, Aliee M, Dudziak D, Merkel R, Smith A-S, Maier A*: Semi-Automatic Cell Correspondence Analysis Using Iterative Point Cloud Registration . 116

P18 *Zhong X, Roser P, Bayer S, Strobel NRN, Birkhold A, Horz T, Kowarschik M, Fahrig R, Maier A*: Pediatric Patient Surface Model Atlas Generation and X-Ray Skin Dose Estimation 122

P19 *Möller A, Maass M, Parbs TJ, Mertins A*: Blind Rigid Motion Estimation for Arbitrary MRI Sampling Trajectories 128

P20 *Preuhs A, Ravikumar N, Manhart M, Stimpel B, Hoppe E, Syben C, Kowarschik M, Maier A*: Maximum Likelihood Estimation of Head Motion Using Epipolar Consistency 134

P21 *Parbs TJ, Möller A, Mertins A*: Retrospective Blind MR Image Recovery with Parametrized Motion Models 140

P22 *Hariharan SG, Kaethner C, Strobel N, Kowarschik M, DiNitto J, Fahrig R, Navab N*: Model-Based Motion Artifact Correction in Digital Subtraction Angiography Using Optical-Flow 146

Software-Demonstrationen

S1 *Scholl I, Bartella A, Moluluo C, Ertural B, Laing F, Suder S*: MedicVR 152

S2 *Stein T, Metzger J, Scherer J, Isensee F, Norajitra T, Kleesiek J, Maier-Hein K, Nolden M*: Efficient Web-Based Review for Automatic Segmentation of Volumetric DICOM Images 158

Session 3: Image Recontruction and Intra-operative Navigation

V10 *Felsner L, Berger M, Kaeppler S, Bopp J, Ludwig V, Weber T, Pelzer G, Michel T, Maier A, Anton G, Riess C*: Abstract: Phase-Sensitive Region-of-Interest Computed Tomography 164

V11 *Droigk C, Maass M, Englisch C, Mertins A*: Joint Multiresolution and Background Detection Reconstruction for Magnetic Particle Imaging 165

V12 *Preuhs A, Maier A, Manhart M, Fotouhi J, Navab N, Unberath M*: Abstract: Double Your Views: Exploiting Symmetry in Transmission Imaging 171

V13 *Breininger K, Hanika M, Weule M, Kowarschik M, Pfister M, Maier A*: 3D-Reconstruction of Stiff Wires from a Single Monoplane X-Ray Image 172

V14 *Hansen L, Diesel J, Heinrich MP*: Regularized Landmark Detection with CAEs for Human Pose Estimation in the Operating Room 178

Postersession 2:

Classification and Detection (Poster)

P23 *Baltruschat IM, Steinmeister LA, Ittrich H, Adam G, Nickisch H, Saalbach A, von Berg J, Grass M, Knopp T*: Abstract: Does Bone Suppression and Lung Detection Improve Chest Disease Classification? 184

P24 *Merten N, Genseke P, Preim B, Kreissl MC, Saalfeld S*: Towards Automated Reporting and Visualization of Lymph Node Metastases of Lung Cancer 185

P25 *Arbogast N, Kurzendorfer T, Breininger K, Mountney P, Toth D, Narayan SA, Maier A*: Workflow Phase Detection in Fluoroscopic Images Using Convolutional Neural Networks 191

P26 *Uzunova H, Ehrhardt J, Kepp T, Handels H*: Abstract: Interpretable Explanations of Black Box Classifiers Applied on Medical Images by Meaningful Perturbations Using Variational Autoencoders 197

P27 *Hagenah J, Heinrich M, Ernst F*: Abstract: Deep Transfer Learning for Aortic Root Dilation Identification in 3D Ultrasound Images ... 198

P28 *Navarro F, Conjeti S, Tombari F, Navab N*: Abstract: Leveraging Web Data for Skin Lesion Classification 199

P29 *Nielsen M, Waldmann M, Frölich A, Fiehler J, Werner R*: Machbarkeitsstudie zur CNN-basierten Identifikation und TICI-Klassifizierung zerebraler ischämischer Infarkte in DSA-Daten 200

P30 *Jain B, Kuhnert N, deOliveira A, Maier A*: Image-Based Detection of MRI Hardware Failures 206

P31 *Xu Y, Schebesch F, Ravikumar N, Maier A*: Detection of Unseen Low-Contrast Signals Using Classic and Novel Model Observers 212

Visualization and Virtual Reality (Poster)

P32 *Maier J, Weiherer M, Huber M, Palm C*: Abstract: Imitating Human Soft Tissue with Dual-Daterial 3D Printing 218

P33 *Leipert M, Sadowski J, Kießling M, Ngandeu EK, Maier A*: A Mixed Reality Simulation for Robotic Systems 219

P34 *Juneja M, Bode-Hofmann M, Haong KS, Meißner S, Merkel V, Vogt J, Wilke N, Wolff A, Hartkens T*: Collecting Image Quality Assessments in Clinical Routine for Deep Learning 225

P35 *von Haxthausen F, Ernst F, Bruder R, García-Vázquez V*: Abstract: HoloLens 231

Imaging and Intra-operative Tracking (Poster)

P36 *Franz AM, Jaeger HA, Seitel A, Cantillon-Murphy P, Maier-Hein L*: Open-Source Tracked Ultrasound with Anser Electromagnetic Tracking 232

P37 *Mittmann BJ, Seitel A, Maier-Hein L, Franz AM*: Navigierte Interventionen im Kopf- und Halsbereich 238

P38 *Ayala L, Wirkert S, Herrera M, Hernández-Aguilera A, Vermuri A, Santos E, Maier-Hein L*: Abstract: Multispectral Imaging Enables Visualization of Spreading Depolarizations in Gyrencephalic Brain . 244

P39 *Li Q, Luckner C, Hertel M, Radicke M, Maier A*: Combining Ultrasound and X-Ray Imaging for Mammography 245

P40 *Mill L, Kling L, Grüneboom A, Schett G, Christiansen S, Maier A*: Towards In-Vivo X-Ray Nanoscopy 251

P41 *Simson W, Paschali M, Zahnd G, Navab N*: Abstract: Beamforming Sub-Sampled Raw Ultrasound Data with DeepFormer 257

P42 *Jäckle S, Strehlow J, Heldmann S*: Shape Sensing with Fiber Bragg Grating Sensors 258

P43 *Felsner L, Hu S, Ludwig V, Anton G, Maier A, Riess C*: On the Characteristics of Helical 3D X-Ray Dark-Field Imaging 264

P44 *Roser P, Birkhold A, Zhong X, Stepina E, Kowarschik M, Fahrig R, Maier A*: Effects of Tissue Material Properties on X-Ray Image, Scatter and Patient Dose 270

P45 *Amri A, Bier B, Maier J, Maier A*: Isocenter Determination from Projection Matrices of a C-Arm CBCT 276

Session 4: Virtual Reality and 3D Modeling

V15 *Engelhardt S, De Simone R, Full PM, Karck M, Wolf I*: Improving Surgical Training Phantoms by Hyperrealism 282

V16 *Hombeck JN, Lichtenberg N, Lawonn K*: Evaluation of Spatial Perception in Virtual Reality within a Medical Context 283

V17 *Kath N, Handels H, Mastmeyer A*: Simulation von Radiofrequenzablationen für die Leberpunktion in 4D-VR-Simulationen 289

V18 *Hagenah J, Evers T, Scharfschwerdt M, Schweikard A, Ernst F*: Abstract: An SVR-Based Data-Driven Leaflet Modeling Approach for Personalized Aortic Valve Prosthesis Development 295

V19 *Eulzer P, Lichtenberg N, Arif R, Brcic A, Karck M, Lawonn K, De Simone R, Engelhardt S*: Mitral Valve Quantification at a Glance 296

Session 5: Registration and Motion Models

V20 *Budelmann D, König L, Papenberg N, Lellmann J*: Fully-Deformable 3D Image Registration in Two Seconds 302

V21 *Rackerseder J, Baust M, Göbl R, Navab N, Hennersperger C*: Abstract: Landmark-Free Initialization of Multi-Modal Image Registration 308

V22 *Hering A, Kuckertz S, Heldmann S, Heinrich MP*: Enhancing Label-Driven Deep Deformable Image Registration with Local Distance Metrics for State-of-the-Art Cardiac Motion Tracking 309

V23 *Geimer T, Ploner SB, Keall P, Bert C, Maier A*: Respiratory Deformation Estimation in X-Ray-Guided IMRT Using a Bilinear Model 315

Session 6: Visible Light

V24 *Aubreville M, Bertram CA, Klopfleisch R, Maier A*: Augmented Mitotic Cell Count Using Field of Interest Proposal 321

V25 *Gessert N, Wittig L, Drömann D, Keck T, Schlaefer A, Ellebrecht DB*: Feasibility of Colon Cancer Detection in Confocal Laser Microscopy Images Using Convolution Neural Networks 327

V26 *Reuter JA, Matuschke F, Schubert N, Axer M*: Efficient Construction of Geometric Nerve Fiber Models for Simulation with 3D-PLI 333

V27 *Yayla M, Toma A, Lenssen JE, Shpacovitch V, Chen K-H, Weichert F, Chen J-J*: Resource-Efficient Nanoparticle Classification Using Frequency Domain Analysis 339

V28 *Wollmann T, Bernhard P, Gunkel M, Braun DM, Meiners J, Simon R, Sauter G, Erfle H, Rippe K, Rohr K*: Black-Box Hyperparameter Optimization for Nuclei Segmentation in Prostate Tissue Images 345

Kategorisierung der Beiträge 351

Autorenverzeichnis 353

Abstract: Anchor-Constrained Plausibility

A Novel Concept for Assessing Tractography and Reducing False-Positives

Peter F. Neher[1], Bram Stieltjes[2], Klaus H. Maier-Hein[1,3]

[1]Division of Medical Image Computing, German Cancer Research Center (DKFZ), Heidelberg, Germany
[2]University Hospital Basel, Radiology & Nuclear Medicine Clinic, Switzerland
[3]Section for Automated Image Analysis, Heidelberg University Hospital, Germany
p.neher@dkfz.de

The problem of false positives in fiber tractography is one of the grand challenges in the research area of diffusion-weighted magnetic resonance imaging (dMRI). Facing fundamental ambiguities especially in bottleneck situations, tractography generates huge numbers of theoretically possible candidate tracts. Only a fraction of these candidates is likely to correspond to the true fiber configuration, posing a difficult sensitivity-specificity trade-off. Current methods address this issue either by focusing exclusively on well-known fiber bundles using prior knowledge or by using tract filtering techniques based on the image signal. Currently, the link between these two choices of purely data driven and prior knowledge based approaches is missing.

We propose a novel concept that rigorously exploits prior knowledge about the existence of anatomically known tracts (anchor tracts) to reduce the degrees of freedom of a successive data-driven filtering of the remaining candidate tracts: anchor-constrained plausibility (ACP). This approach is based on the hypothesis that information about the presence or absence of each anchor influences the plausibility of the candidates and thereby reduces the ambiguities in the problem.

We demonstrate the potential of this concept in a series of phantom experiments: ACP significantly improved the tractography sensitivity-specificity trade-off in such controlled settings (AUC 0.91). The direct assessment of false-positive reduction rates requires a ground truth, which does not exist *in vivo*. *In vivo*, we therefore concentrated on assessing the capabilities of ACP in a structured and objective tractogram analysis of 110 subjects of the Human Connectome Project (HCP) young adult study, providing detailed data-driven insights into what we might be missing when focusing only on anatomically known tracts. This work has previously been published at MICCAI 2018 [1].

References

1. Neher PF, et al. Anchor-constrained plausibility (ACP): a novel concept for assessing tractography and reducing false-positives. Proc MICCAI. 2018;11072:20–27.

Automatic Detection of Blood Vessels in Optical Coherence Tomography Scans

Julia Hofmann[1], Melanie Böge[1], Szymon Gladysz[1], Boris Jutzi[2]

[1]Fraunhofer Institute of Optronics, System Technologies and Image Exploitation (IOSB), Ettlingen
[2]Institute of Photogrammetry and Remote Sensing (IPF), KIT Karlsruhe
julia.hofmann@iosb.fraunhofer.de

Abstract. The aim of this research is to develop a new automated blood vessel (BV) detection algorithm for optical coherence tomography (OCT) scans and corresponding fundus images. The algorithm provides a robust method to detect BV shadows (BVSs) using Radon transformation and other supporting image processing methods. The position of the BVSs is determined in OCT scans and the BV thickness is measured in the fundus images. Additionally, the correlation between BVS thickness and retinal nerve fiber layer (RNFL) thickness is determined. This correlation is of great interest since glaucoma, for example, can be identified by a loss of RNFL thickness.

1 Introduction

Since optical coherence tomography (OCT) offers a noninvasive method for an ophthalmology diagnosis in the fundus area of the eye, this imaging method is of increasing importance. Glaucoma, for example, can be identified by a loss of retinal nerve fiber layer (RNFL) thickness, visible in OCT scans.

The aim of this research is to develop an automated blood vessel (BV) detection algorithm for OCT scans and corresponding fundus images. Recent researches showed reliable results using shadowgraphs to find lateral position and diameter of BVs in 2D OCT-scans. By adding Doppler information, 3D orientation was also obtained [1]. Supervised pixel classification [2] enabled lateral BV detection in OCT 3D volumes. Except manual parameter setting, unsupervised segmentation [3] offered a fully automated segmentation algorithm. Model-based approaches [4, 5] then extended the detection to axial BVs. Efficient automated detection was demonstrated using a deep learning algorithm [6] trained on a specific training data set.

In this research a new automated BV detection algorithm is described without the need of an additional model, training or supplementary data. BVs are visible as vertical shadows in OCT images. This is caused by light absorption through a BV during the OCT procedure. Since the Radon transformation is based on line integrals, vertical lines can be easily reinforced with this method. Together with supporting image processing methods, the approach offers a robust, automated BV shadow (BVS) detection in OCT images. For medical interest a

correlation between BV thickness and RNFL thickness is determined to define a new glaucoma metric.

2 Materials and methods

The data consists of OCT images and corresponding fundus images for each eye. They are recorded as circular and linear scans. Besides the recording mode (circular/linear), the recording density of the single scans (B-scan) can be varied. In this study circular scans and sparse linear OCT images (with 37 B-scans) from 16 participants and dense linear OCT images (with 193 B-scans in the recording area and a density of 30 μm) from 12 participants are included.

2.1 Methodology

The different data types are processed with the same operational sequence (Fig. 1) which was developed for 2D data. The processing steps are described in this section. Afterwards, a description of the process in case of 3D data is given.

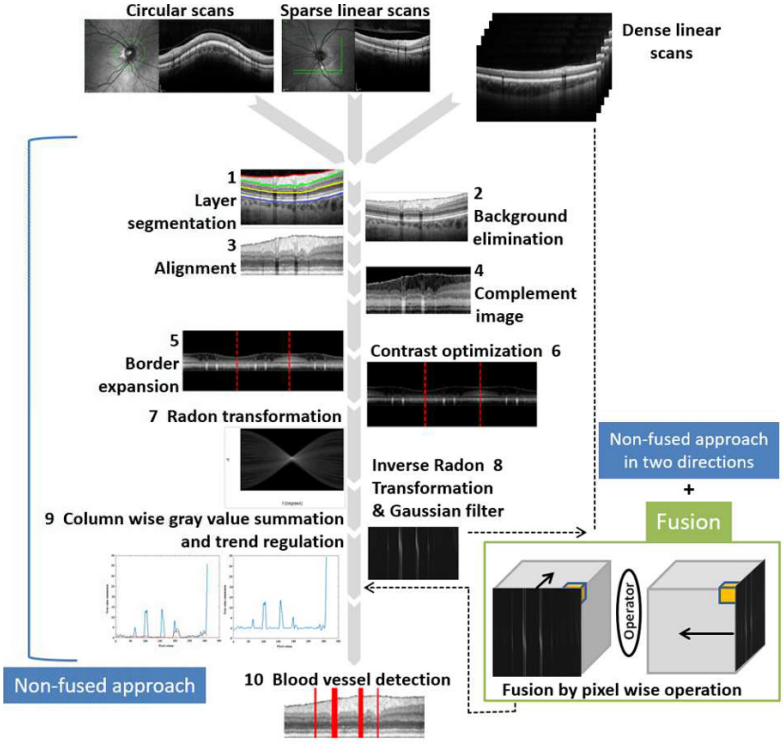

Fig. 1. Flowchart of the proposed approach.

Preparatory steps for the radon transformation The first process step is the layer segmentation (1). For background elimination (2) all values above the top layer, Inner Limiting Membrane (ILM), are set to the maximum gray value to ensure maximum contrast for the BVSs. For alignment (3) each column (A-scan) in the OCT image is shifted up or down according to the Retinal Pigment Epithelium layer (RPE) as baseline. This step simplifies cropping of the image to the area of interest, which suppresses the influence of noise from surrounding areas. Layer segmentation and alignment are applied with functions created by Mayer et al. [7]. At this point in the process BVSs have low gray values which are hard to reinforce. For this reason, a negative image (4) is produced to enable an amplification of the bright BVSs. Border expansion (5) and contrast optimization (6) are part of the boundary problem step. They will be explained after the Radon transformation.

Radon transformation Since the BVSs in OCT scans are vertical lines, a line detection algorithm is beneficial for this application. The Radon transformation (7) is a linear integral transformation defined by Johann Radon [8]. For the transformation to Radon space, each pixel will be represented in polar coordinates (ρ, θ). The rotation and translation starts from the origin of the image coordinate system. For each angle θ and each distance ρ the intensities of the image are summed up. The result is $r(\rho, \theta)$, consisting of the column gray value summations in all orientations. We assume that the BVSs are the only vertical lines in the OCT images. They can be seen in Radon space in the zero degree column. For easier and more robust BVS detection, the BVSs are reinforced. To enhance the contrast of BVSs in the original image, all values in the first column in Radon space are squared. The following columns are attenuated by multiplying all values with a sloping function. BVSs might not be exactly vertical and therefore to maintain slightly slant shadow areas, small angles are less attenuated than line integrals of higher angles. We found that the sloping exponential function was most suitable for reinforcement. It falls very steeply which causes stronger attenuation in the columns of higher angles. After the relevant columns in Radon space are amplified, the image is transformed back to the image format with the inverse Radon transformation.

Boundary problem The inverse Radon transformation causes artifacts at the border areas of the image which leads to false BVS detections. The origin of this can be explained using the concept of spatial frequency Fourier transformation. Frequencies are expected to be infinite and the border areas of the finite image can therefore not be reconstructed with the inverse Radon transformation. To avoid this, a border expansion (5) by flipping the whole image on both sides is applied. Also, a threshold is used to optimize contrast (6) and get rid of disturbing insignificant values. Darker values on the right boundary arise during the OCT recording and cause falsely detected BVSs. To remove this trend (9) a 15 x 15 pixel window is shifted along the graph. The mean values of the window values are subtracted from the original summation values.

Blood vessel shadow detection After these image processing steps, the BVSs can be detected in the trend-regulated gray value summation graph. For the BVS detection a quantile threshold is calculated from the graph.

Thickness measurement The BVSs visible in the OCT data do not necessarily correspond to the real BV thickness. Often the scan corresponds to a diagonal cut through the BV. The position of a BVS is therefore transferred to the fundus image. Here, a diameter measurement is performed by generating a BV-filling circle around the detected position.

Pseudo-3D processing - fusion after bidirectional processing The acquisition density of the B-scans corresponding to the dense linear data is too sparse to allow a true 3D processing. For that reason, a pseudo 3D processing (fusion) is applied to approximate a volumetric processing and gain an anisotropic detection. For a volumetric approximation all dense linear scans consecutively are approximated as a cube (Fig. 2). The dense linear scans are concatenated and A-sheets are generated. The A-sheets consist of the same A-scan column in each B-scan. In the x-, y-, z-coordinate system (Fig. 2), they consist of one y-z plane for each x. The pixel size varies between B-scans (4×4 μm) and A-sheets (30×4 μm) according to the acquisition density of 30 μm. After the generation of the A-sheets, the whole non-fused approach is performed separately for all B-scans and all A-sheets. This way the processing is performed for two directions giving two resultant cubes. The cubes are fused with pixel-wise averaging of the pixel values. After the fusion, the BVS detection is applied similarly to the non-fused approach (Fig. 1).

Evaluation A comparison of BVS detections to ground truth is presented. Manual detections by an expert ophthalmologist are used as ground truth in all evaluations. The consistency of the BVS thickness measurements between ground truth and the developed approach was validated using the root mean square error (RSME). This metric defines the deviation between the expected

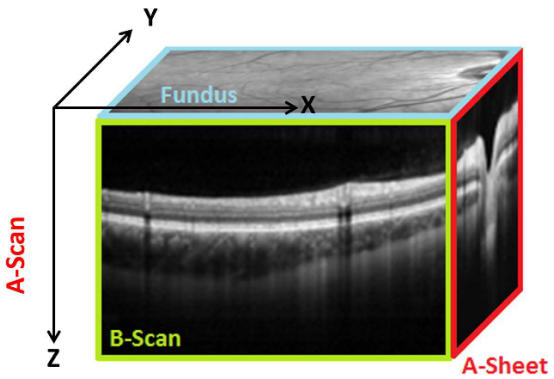

Fig. 2. Coordinate system of the OCT images.

Table 1. Table of results and comparison values.

	Radon approach (all data)	Radon approach (dense scans)		OCTSeg (all data)	OCTSeg (dense scans)
Detection rate	90%	90%	89%	90%	85%
RMSE (pixel)	5.16	5.32	5.44	3.25	8.24

value and the measurement. It provides information about the accuracy of the measurements.

Glaucoma causes RNFL thinning. It might also effect BV thickness. For this reason the correlation of the layer thickness and BV thickness is of interest for ophthalmology. It is tested if the correlation generated from patients suffering from glaucoma shows significant differences in comparison to the correlation obtained from healthy eyes. Only ground truth layer segmentation and BVS detections of sparse OCT scans are used for the correlation estimation to avoid influence of false detections. Correlation can only be determined for detected BVSs without transfer to the fundus image (Sec. Thickness measurement), since for glaucomatous eyes, only OCT scans and not fundus images are available in the data set.

3 Results

The experiments involved sparse linear scans and circular scans from 16 participants and 241 dense linear scans.

The detection rates and thickness accuracies are given in Tab. 1. All detections were compared to the approach of Mayer [7] (OCTSeg). The proposed algorithm is able to achieve the same detection rate as OCTSeg. On the dense linear scans the Radon approach even outperforms the fusion approach and OCTSeg. Regarding all data, OCTSeg achieves the best thickness measurement accuracy. On the dense linear scans the Radon approach performs best. As shown in Tab. 3, the RNFL thickness for the healthy eyes is immensely higher than for glaucomatous eyes. As expected, the RNFL thickness is a significant criteria for glaucoma identification. The measured BV thickness maxima on the other hand only differ 3 μm. The BV thickness or the correlation between BV thickness and RNFL thickness is therefore not beneficial as glaucoma metric.

	Maximum RNFL thickness (μm)	Maximum BV thickness (μm)
Glaucomatous eyes	72	38
Healthy eyes	252	41

Table 2. Correlation of RNFL thickness and BV thickness.

4 Discussion

The advantage of the proposed BV detection algorithm is that no model, training or supplementary data is needed. The results described in this paper show that a sufficient BVS detection rate is enabled with the non-fused, and also the fusion approach. Since the resolution varies according to the recording direction, the fusion detection is not as dense as the radon approach and therefore achieves a lower detection rate. With the transfer to the fundus image (Sec. Thickness measurement) a reliable BV thickness measurement is demonstrated. A metric for glaucomatous eyes could be found, even if the RNFL thickness is more significant for glaucoma than the BV thickness. Here, an additional data acquisition of OCT scans with corresponding fundus images on glaucomatous eyes should be performed to enable a meaningful correlation of layer thickness and BV thickness. Layer segmentation in the approach influences the detection. In the future, a greater independence from the layer segmentation approach (here taken of OCTSeg) will be sought. In further research, the approach could be compared with OCT Angiography to additionally prove the effectiveness.

References

1. Wehbe H, Ruggeri M, Jiao S, et al. Automatic retinal blood vessel parameters calculation in spectral domain optical coherence tomography. Procs SPIE. 2007;6429:6429–1–7.
2. Niemeijer M, Garvin MK, van B Ginneken, et al. Vessel segmentation in 3D spectral OCT scans of the retina. Procs SPIE. 2008;6914:6914–1–8.
3. Annunziata R, Garzelli A, Ballerini L, et al. Leveraging multiscale hessian-based enhancement with a novel exudate inpainting technique for retinal vessel segmentation. IEEE J Biomed Health Inform. 2016;20(4):1129–38.
4. Lee KM. Segmentations of the Intraretinal Surfaces, Optic Disc and Retinal Blood Vessels in 3D-OCT Scans. Iowa: Univ Iowa; 2009.
5. Pilch M, Wenner Y, Strohmayr E, et al. Automated segmentation of retinal blood vessels in spectral domain optical coherence tomography scans. Biomed Opt Expr. 2012;3(7):1478–91.
6. Li Q, Fengi B, Xie L, et al. A cross-modality learning approach for vessel segmentation in retinal images. IEEE Trans Med Imaging. 2016;35(1):109–18.
7. Mayer MA, Hornegger J, Mardin C, et al. Retinal nerve fiber layer segmentation on FD-OCT scans of normal subjects and glaucoma patients. Biomed Opt Expr. 2010;1(5):1358–83.
8. Radon J. Über die Bestimmung von Funktionen durch Ihre Integralwerte Längs Geweisser Mannigfaltigkeiten. Berichte Sächsische Acad Wissenschaft Math Phys, Klass. 1917;69:262.

Prediction of Liver Function Based on DCE-CT

Oliver Rippel[1], Daniel Truhn[2], Johannes Thüring[2], Christoph Haarburger[1], Christiane K. Kuhl[2], Dorit Merhof[1]

[1]Institute of Imaging & Computer Vision, RWTH Aachen University, Germany
[2]Department of Diagnostic and Interventional Radiology, University Hospital Aachen, Germany
oliver.rippel@lfb.rwth-aachen.de

Abstract. Liver function analysis is crucial for staging and treating chronic liver diseases (CLD). Despite CLD being one of the most prevalent diseases of our time, research regarding liver in the Medical Image Computing community is often focused on diagnosing and treating CLD's long term effects such as the occurance of malignancies, e.g. hepatocellular carcinoma. The Child-Pugh (CP) score is a surrogate for liver function used to quantify liver cirrhosis, a common CLD, and consists of 3 disease progression stages *A*, *B* and *C*. While a correlation between CP and liver specific contrast agent uptake for dynamic conrast enhanced (DCE)-MRI has been found, no such correlation has been shown for DCE-CT scans, which are more commonly used in clinical practice. Using a transfer learning approach, we train a CNN for prediction of CP based on DCE-CT images of the liver alone. Agreement between the achieved CNN based scoring and ground truth CP scores is statistically significant, and a rank correlation of 0.43, similar to what is reported for DCE-MRI, was found. Subsequently, a statistically significant CP classifier with an overall accuracy of 0.57 was formed by employing clinically used cutoff values.

1 Introduction

Assessing liver function is crucial for staging and treating chronic liver diseases (CLD) [1]. Due to its various functions, there exist a multitude of tests to assess liver state [2], some of them based on imaging. A very common clinical scoring system of liver function is the Child-Pugh score (CP) [3]. It scores several important indicators such as e.g. ascites and subsequently aggregates them. CP classes are then gained by applying the following thresholds: CP *A* 5-6 points, CP *B* 7-9 points, and CP *C* 10-15 points. The CP score is clinically used to assess the prognosis of liver cirrhosis, a CLD responsible for more than 1 million deaths annually [4], and monitor its transition to the end stage.

In the Medical Image Computing community, research on CP so far has been focused on Dynamic Contrast Enhanced-MRI (DCE-MRI). Here, Motosugi et al. [5] have shown an association between CP score and accumulation of liver specific contrast agent, as confirmed by further literature [6, 7]. Moreover, a successful prediction of liver fibrosis was performed by Yasaka et al. [8], again

based on the accumulation of liver specific contrast agent in DCE-MRI. To the best of our knowledge, successful evaluation of liver function based on DCE-CT has not been reported yet, irrespective of the widespread use of DCE-CT in clinical practice as a routine examination.

The main contribution of our work is an approach for predicting CP scores based on DCE-CT imaging alone, using a combination of state-of-the-art convolutional neural networks (CNN) with transfer learning.

2 Methods

2.1 Dataset

In total, the dataset comprises 259 subjects (76 CP score A, 120 CP B, 63 CP C). For each subject, a radiologist with more than 3 years of experience in abdominal imaging reviewed automatic liver delineation in the venous phase generated by Philips Intellispace.

CT imaging was performed by using helical CT scanners (Somatom Definition Flash and Somatom Definiton AS, Siemens Medical Sysems, Forchheim, Germany). The scans were acquired in a craniocaudal direction by using a detector configuration of 128 or 40 x 0.6 mm, a tube current of 120 kVp, quality reference of 240 mAs, and online dose modulation in all phases (pitch 1.0), during a single breath-hold helical acquisition of roughly 10 seconds (slightly varying due to the differing liver sizes). For all imaging, the gantry rotation speed was 2 Hz. The contrast-enhanced images were created with a weight-adjusted application of iodinated contrast material (1.5 mL per kilogram of body weight; Iopramide 370 mg/mL, Ultravist, Shering, Germany) administered at a rate of 3 mL/s by power injector. Subsequently the non-enhanced (native) as well as arterial and venous phases were acquired. The acquisition of the arterial phase started 6 seconds after the automatic detection of peak aortic enhancement at the level of the coeliac trunk with a threshhold of 140 HU; portal venous phase was scanned 55 seconds after the start of the contrast injection. Image reconstruction was performed with axial 1-mm images, an increment of 0.7 mm, and a B30f convolutional kernel for all phases (Fig. 1, representative axial slices).

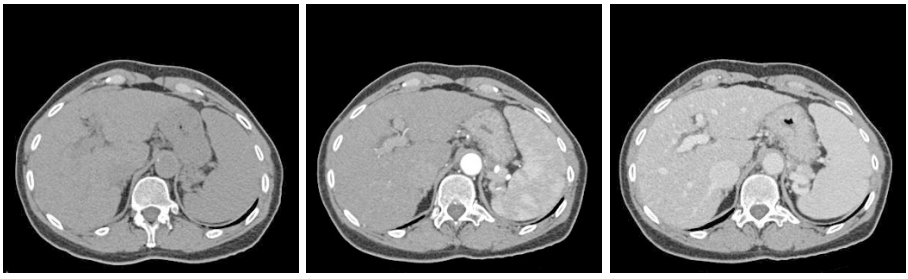

(a) non-contrast enhanced (b) arterial enhancement (c) venous enhancement

Fig. 1. Representative images of a contrast enhanced liver CT-scan. Images were reconstructed with a B30f kernel in soft-tissue-window.

2.2 Pre-processing

First, native and arterial phases were registered to the venous phases with a rigid registration algorithm under the assumption that liver shape would be constant in all three phases. Registration itself was performed using SimpleElastix [9] with default parameters. Subsequently, voxel intensities were linearly mapped to a soft tissue window (center 40 HU, width 400 HU).

Next, axial patches of 224x224 in-plane dimension were extracted around the centerpoint of the liver along 20 % to 80 % of its craniocaudal extension. This approach has the advantage of incorporating the context around the liver in a patch, and may thus capture effects such as ascites. Furthermore, it reduces the need for resizing, as axial patch dimensions are concordant with the input shape expected by the pretrained model. In total, 12492 patches were extracted in this manner to be used for model finetuning.

2.3 Model architecture and training

For the model architecture, a ResNet18 [10] pretrained on ImageNet [11] was used in a transfer learning approach [12]. At its core, ResNet consists of residual blocks, where deviations from an identity mapping are learned by the model. This has been shown to sucessfully tackle the problem of vanishing gradients inherent to deep CNNs. While model depth of a ResNet architecture can be arbitrary, we use a depth of 18, minimizing the number of trainable parameters and therefore risk of overfitting.

The output of the pretrained ResNet18 model was adapted to our ordering problem, giving a single continous value for every slice. By stacking the three phases of the CT scan, the number of input channels satisfy the number of channels as required by the pretrained model. While modifications to the axial dimensions are not necessary, on-the-fly data augmentation was used to reduce overfitting of trained models. These consisted of rotation, scaling, as well as elastic deformation and were performed by the batchgenerators framework[1]. Model finetuning on the CT images itself was performed using an L2-regularized Adam optimizer with initial learning rate of 0.0005 and a decay rate of 0.5 every 10 epochs and L2-penalty of 0.001. All layers were trained simultaneously, employing the MeanSquareError (MSE) metric for training and the accuracy metric for validation. MSE was chosen over a classification loss function, such as e.g. CrossEntropy, to reflect the ordinal nature of the CP score. For this, class labels were assigned based on the clinically used thresholds: [5, 6] for CP *A*, [7, 9] for CP *B* and [10, 15] for CP *C*. As the output of the model is continuous, values are rounded to the nearest integer to yield CP class predictions.

The model was trained using 10 fold cross-validation. For each fold, patches are split into training, validation and test set such that patches from a single patient are exclusively included in either training, validation or test set. The splitting ratios were 0.63, 0.27 and 0.1 for training, validation and test sets,

[1] https://github.com/MIC-DKFZ/batchgenerators